

Article

Numerical Analysis of Transient Burn Injury Grading Through Coupled Heat Transfer and Damage Integral Modeling

Chao Zhang ¹, Xinbin Ma ¹, Mengxi Li ², Yubin Qiu ¹, Moon Keun Kim ³  and Jiying Liu ^{1,*} 

¹ School of Thermal Engineering, Shandong Jianzhu University, Jinan 250101, China; zhangchao19@sdjzu.edu.cn (C.Z.)

² School of Modern Design, Shandong University of Engineering and Vocational Technology, Jinan 250200, China

³ Department of Built Environment, Oslo Metropolitan University, N-0130 Oslo, Norway

* Correspondence: jxl83@sdjzu.edu.cn

Abstract: The accurate assessment of parameters such as burn degree, volume, and depth is a prerequisite for the effective treatment of patients. However, as an unsteady heat transfer process, the temperature of the burn damage volume changes over time, and it is difficult to accurately calculate the integral value of the damage, which is used to assess the burn degree. Therefore, it is impossible to accurately determine the location and volume of damage at all burn degrees. In this study, the C language is used to program a user-defined function of the burn damage integral formula, and the coupled numerical simulation method is used to calculate the heat transfer and damage in a high-temperature water burn process. Then, the temperature and burn damage integral value of each point can be determined to accurately assess and distinguish the burn degree in real time, and estimate the position distribution, volume size, and transient change trend of each burn degree. Under the working conditions selected in this paper, the heat source mainly affects the epidermis and dermis directly below, and has less influence on the area above, which is in convective heat transfer. The damage integral value is very sensitive to temperature, and the highest damage integral value caused by 373 K is two and four orders of magnitude higher than that of 363 K and 353 K, respectively. The increase in the heat source temperature caused the volume of a third-degree burn to increase rapidly in the early stage of injury, but the volume of second-degree and first-degree burns did not change much. After heating at 373 K for 15 s and delaying the action for 45 s, the volume of first-, second-, and third-degree burns accounted for 0.4, 2.9, and 1.9%, respectively, and the total volume of damage accounted for only 5.2% of the total volume.



Academic Editor: Jean-Noël Jaubert

Received: 6 November 2024

Revised: 16 January 2025

Accepted: 28 January 2025

Published: 4 February 2025

Citation: Zhang, C.; Ma, X.; Li, M.; Qiu, Y.; Kim, M.K.; Liu, J. Numerical Analysis of Transient Burn Injury Grading Through Coupled Heat Transfer and Damage Integral Modeling. *Thermo* **2025**, *5*, 4. <https://doi.org/10.3390/thermo5010004>

Copyright: © 2025 by the authors. Licensee MDPI, Basel, Switzerland. This article is an open access article distributed under the terms and conditions of the Creative Commons Attribution (CC BY) license (<https://creativecommons.org/licenses/by/4.0/>).

Keywords: burn degree; transient defined function; numerical simulation; heat transfer; transient variation characteristics

1. Introduction

There are an estimated 11 million patients with burns requiring medical treatment each year [1]. Every year, more than 265,000 people worldwide die of burn injuries and nearly 10% of child deaths are burn-related [2,3]. Millions more worldwide suffer from burn-related diseases, especially disability and disfigurement, which have negative psychological, social, and economic consequences for survivors and their families. The median total cost per burn patient was EUR 26,540 within the first three months of injury [4]. Furthermore, burns are more prevalent in people of low socioeconomic status. Survivors will be poorer than they were pre-injury according to a survey [5]. Due to the negative effects of burn

injury, pathophysiology, biothermal theoretical studies, and the development of novel therapeutic drugs have attracted significant attention from medical experts and researchers in recent years.

Since the introduction of the Pennes bioheat transfer equation (PBTE), it has been differentiated between the bioheat transfer problem and the heat transfer problem of engineering materials on a fundamental level [6]. The PBTE is widely used due to its straightforward calculation, but it usually deviates somewhat from the actual situation. Diller et al. made an outstanding contribution using the PBTE to demonstrate that post-burn cooling is not a thermal effect only, but also largely relies on biological effects [7]. In parallel with the development of theoretical studies, animal experiments on burns are being conducted at present. Rat models of burn injuries began to be used in 1946 [8]. Since then, pig [9–11], mouse [12–14], and rabbit [15–18] models have been developed to study the molecular biology, cell biology, and pathophysiology of burns. The PBTE and animal burn injury models contribute to promote an in-depth understanding of burn injuries, leading to significant advances in the treatment of burns, such as keratinocytes and stem cells [19,20], wound coverage, and transplantation [21–24].

However, the specific treatment strategy for burns depends on the depth, location, and burn degree. The temperature, location, action time of the heat source, and cooling time all have a significant effect on these burn parameters [25–27]. Since most burn experiments can only be performed on animals, and there is a certain difference between them and human burns, the burn degree is difficult to determine quantitatively. With the development of computer-aided technology, more and more numerical simulation methods are being used in burn research. Ng and Chua performed numerical modeling and a parametric sensitivity analysis of post-burn skin prediction [28–30]. John et al. studied the extent and depth of burn injury by numerical calculation and graded the injury with values [31]. Dai et al. modified the Pennes model and developed a mathematical model to assess radiation heating-induced skin burn injury [32]. Ng et al. studied heat transfer processes during burns and provided temperature distributions and the extent of burn injury [33,34]. Jiang et al. developed a one-dimensional multilayer model to predict the effects of thermal physical properties and geometrical dimensions on the transient temperature and damage function distributions [35]. Mohamad et al. used COMSOL Multiphysics[®] software v5.6 to evaluate the effect of heat flux distribution and internal heat generation on the thermal damage in multilayer tissue during thermotherapy. However, the distribution accuracy of the burn degree needs to be further improved [36]. Kashcooli et al. developed a model including a counter-current multilevel vessel network and a three-dimensional (3D) triple-layered skin structure, and used it to investigate the effects of different parameters on temperature distribution [37]. Lee et al. numerically calculated the heat transfer in a unit of 3D skin tissue with an embedded vascular system of actual histological structure and obtained the tissue temperature and blood temperatures in artery and vein vessels [38]. Wang et al. studied the effects of fractal vascular trees on tissue temperature and intracellular ice formation during combined cancer therapy with cryosurgery and hyperthermia using a 3D numerical simulation model. They used the thermal and cryo damage functions together with the injury caused by intracellular ice formation to evaluate the killing effect [39]. Shirkavand et al. used numerical simulation to study the effects of blood perfusion and body metabolism on the temperature profile of the human forearm in hyperthermia conditions [40]. Muddassir et al. developed a 3D physics-based numerical model of laser–skin interactions to predict the temperature distribution and thermal damage [41]. A multi-segmented human bioheat model was developed by Wu et al. to study the heat transfer process of the human body in extremely cold environments [42]. Dinda et al. developed a MATLAB-based numerical model to

evaluate the temperature data in an anisotropic medium like human skin [43]. Log has performed a lot of numerical simulation work on skin burns, including direct burn by hot rice porridge spills, burn by hot coffee under clothes, and flame exposure of pre-cooled skin [44–46]. Many other scholars have also performed numerical calculations of heat transfer and the burn damage integral value (Ω) in the process of skin burns [47–50]. However, most of the existing research described above focuses on the heat transfer during the burn process, and the calculation accuracy of the burn damage integral value Ω is somewhat lacking, and there is no research on the real-time changes in the burn degree, location, volume, and other parameters during the burn process. The reason is that in the heat transfer process of burns, the temperature of each grid in the calculation area may be different from other grids and may change over time. When the number of grids is particularly large, it is difficult to accurately monitor and calculate the temperature and burn damage integral value of each grid cell.

In the existing literature, most of the studies can give the temperature distribution of the burn area, but almost none of them can give the regional distribution of burn grades and their dynamic changes over time. In this study, to accurately determine the location and volume of damage at all burn degrees, the C language is used to program a user-defined function of the damage integral formula, and the coupling numerical simulation method is used to calculate the heat transfer and damage in a high-temperature water burn process. Subsequently, the temperature and burn damage integral value Ω of each point can be obtained to accurately assess and distinguish the burn degree in real time, and predict the position distribution, volume size, and transient change trend of each burn. The results of this study can be applied to the clinical diagnosis of burns and quickly and accurately assess the burn degree, depth, volume, and other parameters based on the burn process, thus providing a reliable basis for the next step of successful treatment. If the UDF used in this paper is not used, it is difficult to accurately monitor the temperature change of each grid in the calculation area with a large number of grids or a working condition with complex heat transfer, and it is even more difficult to accurately calculate the burn integral value and divide the burn grades.

2. Numerical Description

According to previous studies, the burn degree can be calculated and assessed by the damage integral formula. However, the integral value is very sensitive to temperature, and a skin burn is an unsteady heat transfer process; thus, it is difficult to analytically calculate the integral value of the damage. As a result, there are few studies that can provide the change law of the integral value of skin damage in the process of burn injury, let alone the transient variation characteristics of parameters such as the position and volume of the burn damage at all levels. In this study, the C language is used to program a user-defined function of the damage integral formula, and the coupling numerical simulation method is used to calculate the heat transfer and damage during a high-temperature water burn process. Then, the temperature and burn damage integral value Ω of each point can be obtained to accurately assess and distinguish burn degrees in real time, and predict the position distribution, volume size, and transient change trend of each burn degree. The technology roadmap used for the calculations in this study is shown in Figure 1.

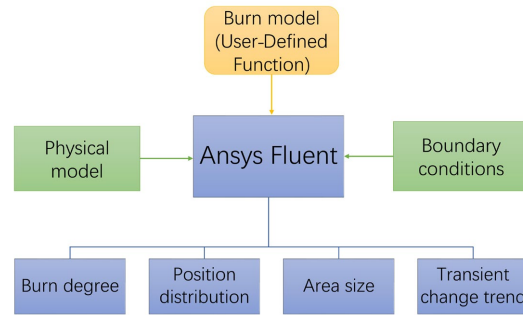


Figure 1. Technology roadmap used for the calculations in this study.

2.1. Physical Model

Accurate measurement of the grid node temperature is the premise of calculating the burn damage integral value Ω . To obtain accurate numerical calculation results, the establishment of a physical model and grid system is very important. A 3D cylinder with a diameter of 20 mm and a height of 12.1 mm (the sum of the thickness of the epidermis, dermis, and subcutaneous tissue) was used as the research object. The shape of the heat source was simplified as a disk with a diameter of 10 mm applied on the top. The 3D model can be simplified into a two-dimensional axisymmetric model using the axisymmetric relationship, as depicted in Figure 2, which shows the muscle tissue under the three layers of skin together, although it is not the calculation area in this study. Also indicated in this figure are the six points for subsequent calculation and monitoring. The height direction is located at the center of each layer of skin, and the radial direction is located just below the center of the circle and at the border. According to the law of heat transfer, when the heat source is applied, the heat is transferred in the downward and lower right direction, and the skin in the atmospheric environment loses heat to the environment. The schematic diagrams of these two types of heat transfer are also shown in Figure 2. Since this numerical model needs to accurately calculate the burn damage integral value Ω of each grid node, the calculation area is finely divided into grids, and individual areas are encrypted. The schematic diagram of the grid in some areas is also shown in Figure 2. To ensure the accuracy of the calculation results, several grid division methods were used for grid independence verification, and it was found that the calculation data tended to be stable when the total number of grids reached about 250,000, so this grid system was used in subsequent calculations.

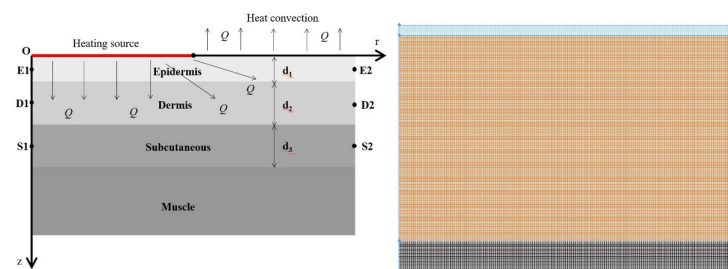


Figure 2. Schematic diagrams of the computational regions and the grid system (The red line indicates the heating source in the 2D model).

2.2. Governing Equation

In human tissue, both blood perfusion and metabolism generate heat transfer, and the general 3D heat transfer governing equation in the cylindrical coordinate system can be expressed as follows:

$$\frac{\partial(\rho_s c_s T)}{\partial \tau} = \frac{1}{r} \frac{\partial}{\partial r} \left(\lambda_s r \frac{\partial T}{\partial r} \right) + \frac{1}{r^2} \frac{\partial}{\partial \varphi} \left(\lambda_s \frac{\partial T}{\partial \varphi} \right) + \frac{\partial}{\partial z} \left(\lambda_s \frac{\partial T}{\partial z} \right) + Q_b + Q_{met} \quad (1)$$

where ρ_s , c_s , and λ_s are the density, specific heat of skin tissue, and thermal conductivity of tissue, respectively. Q_b and Q_{met} are the heat generated by blood perfusion and metabolism, respectively. The blood perfusion heat transport Q_b can be calculated by the following equation:

$$Q_b = \omega_b \rho_b c_b (T_b - T) \quad (2)$$

where ω_b , ρ_b , c_b , and T_b are the blood perfusion rate, density, specific heat of blood, and temperature of blood, respectively.

Since the heat exchange effect caused by blood perfusion is very weak and generally ignored in other studies, this heat exchange effect is not considered in this study. The temperature of the heat source used in the calculation model is relatively high, and since the heat transfer to the inside of the human tissue is much higher than the heat generated by metabolism, Q_{met} could also be ignored in this model.

Besides the heat transfer to the inside of the tissue, this calculation model also includes the natural convection heat dissipation between the skin surface and the external atmospheric environment. When the heat source with a radius of r_{hs} is active for a time τ_{hs} , only the area outside the heat source is in convective heat exchange, and when the heat source is withdrawn, the entire skin surface is in convective heat exchange. Therefore, for the skin surface at $z = 0$, the heat transfer equation can be expressed as follows:

$$-\frac{\partial(\lambda_s T)}{\partial z} = h(T - T_\infty) \begin{cases} 0 \leq \tau < \tau_{hs} \text{ and } r > r_{hs} \\ \tau \geq \tau_{hs} \text{ and } r \geq 0 \end{cases} \quad (3)$$

where h is the natural convection heat transfer coefficient and T_∞ is the ambient temperature of the atmosphere.

2.3. Burn Model

In order to accurately determine the degree of burns, Henriques developed a mathematical model for calculating the burn damage integral value Ω based on the Arrhenius equation, which can be used to determine the degree of burns according to different integral values. The mathematical equation is expressed as follows [44]:

$$\Omega = \begin{cases} \int_0^\tau P \exp\left(-\frac{\Delta E}{RT}\right) dt & T \geq 310.15K \\ 0 & T < 310.15K \end{cases} \quad (4)$$

where P is the pre-exponential frequency factor, ΔE is the activation energy, and R is the molar gas constant. The values of these parameters will be given later. From the damage integral calculation formula, it can be seen that no damage occurs when the tissue temperature is lower than 316 K, and when the temperature exceeds this value, the burn damage integral value Ω is not only related to temperature, but also related to the action time. However, since the burn process involves unsteady heat transfer, and the temperature of the damaged part is constantly changing, it is difficult to obtain this value analytically. Therefore, this study embeds the damage integral function Equation (3) into the ANSYS FLUENT 2020R1 as a user-defined function with the help of C language programming, simultaneously calculates the heat transfer equation and burn damage integral value Ω for each grid node, and obtains the change law of temperature and burn damage integral value Ω at each point of each layer, which is used to accurately judge and distinguish the burn degree during the burn process in real time. Although Equation (4) has appeared in many studies, it is difficult to apply it to numerical simulation calculations. This is because in the heat transfer process, the temperature of each grid in the calculation area may be different from other grids and may change over time. When the number of grids is

particularly large, it is difficult to accurately monitor and calculate the temperature and burn damage integral value of each grid cell. This article uses UDF programming to achieve this function more easily. Numerical calculations can be performed for each tiny grid, so the burn damage integral value Ω can be accurately determined for each grid point. According to the literature, when the burn damage integral value Ω is in the range of 0.53~1, the tissue corresponds to a first-degree burn; when Ω is in the range of 1~10,000, the tissue corresponds to a second-degree burn; and when Ω is higher than 10000, it corresponds to a third-degree burn.

2.4. Parameter Determination and Boundary Conditions

The physical parameters of skin tissue are very important to the numerical calculation. The data selected for the model in this study are basically consistent with those reported in the literature, which are shown in Table 1.

Table 1. Physical parameters of each layer of skin tissue.

Physical Parameters	Epidermis	Dermis	Subcutaneous
Density ρ_s , kg/m ³	1200	1200	1000
Specific heat c_s , J/(kg·K)	3600	3600	2500
Thermal conductivity λ_s , W/(m·K)	0.22	0.4	0.2
Thickness d , mm	0.1	2	10

This study also includes the calculation of the damage integral function and the solution of the convective heat transfer. The relevant parameters used are shown in Table 2.

Table 2. Other parameters used in the numerical model.

Parameters	Symbol	Unit	Value
Pre-exponential frequency factor	P	s ⁻¹	3.1×10^{98}
Activation energy	ΔE	J·mol ⁻¹	6.28×10^8
Molar gas constant	R	J·mol ⁻¹ ·K ⁻¹	8314
Convection transfer rate	h	W·m ⁻¹ ·K ⁻¹	10
Ambient temperature	T_∞	K	293.15
Radius of heat source	r_{hs}	mm	5
Radius of physical model	r_{pm}	mm	10
Thickness of physical model	z_{pm}	mm	12.1

The model calculation process in this study is an unsteady process, and the initial body temperature is set at a constant temperature of 310.15 K. Thus, the initial condition is as follows:

$$T_i = 310.15 \text{ K} \quad (5)$$

For $z = 0$, that is, the boundary conditions of the skin surface, refer to Equation (3); other boundaries are adiabatic conditions, which can be expressed as a mathematical formula, as follows:

$$\begin{cases} \frac{\partial T}{\partial r} = 0 & r = 0 \& 0 \leq z \leq -z_{pm} \\ \frac{\partial T}{\partial r} = 0 & r = r_{pm} \& 0 \leq z \leq -z_{pm} \\ \frac{\partial T}{\partial z} = 0 & z = -z_{pm} \& 0 \leq r \leq r_{pm} \end{cases} \quad (6)$$

2.5. Description of Working Conditions

According to the damage integral formula, the damage integral value Ω changes drastically at high temperatures. To capture the transient change law of the process, this study uses hot water at 353, 363, and 373 K as a constant-temperature heat source, and an

action time of 5, 10, and 15 s, respectively. Therefore, there are nine combined working conditions in total, as shown in Table 3.

Table 3. Working conditions and parameters.

Working Conditions	Water Temperature, K	Action Time, s
Case1	353	5
Case2	353	10
Case3	353	15
Case4	363	5
Case5	363	10
Case6	363	15
Case7	373	5
Case8	373	10
Case9	373	15

3. Numerical Results and Discussion

3.1. Validation Using Published Data

In order to accurately calculate the real-time damage integral value Ω of each element node in the numerical model, the C programming language was used in this study to program the damage integral function, which was then loaded into the numerical calculation model in the form of a user-defined function. The accuracy of the model established in this study was verified by numerically calculating the physical model developed by Log [44–46] to obtain the temperature and damage integral characteristics, which were compared with the data in the literature; the results shown in Figure 3 revealed that the numerical calculation model established in this study can not only predict the temperature change more accurately, but also calculate the damage integral value Ω more accurately. Because our calculation model takes into account the heat dissipation at non-heat sources, the temperature and burn integral values at the same monitoring location should be lower to match the actual working conditions. Therefore, it is reasonable to assume that the numerical calculation model established in this paper can be applied to the study of heat transfer and burn injury characteristics in subsequent simulation studies.

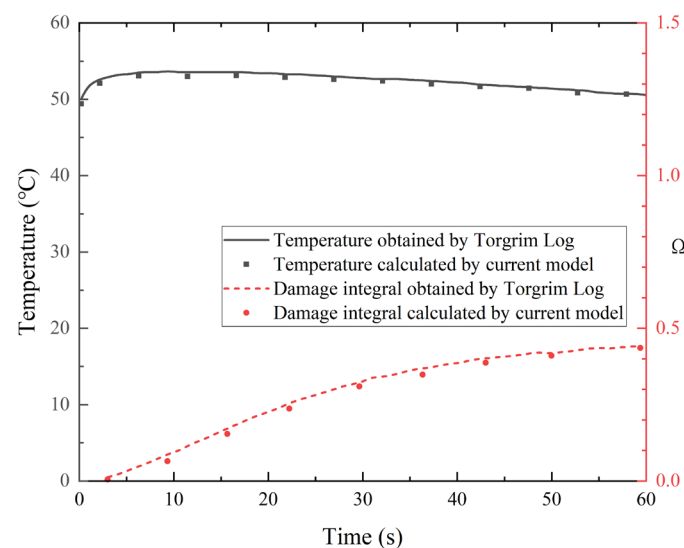


Figure 3. Comparison of numerical model calculation data to literature data.

3.2. Effect of the Heat Source on the Temperature Distribution

The temperature profile curve of each point in each case can be obtained after performing temperature monitoring on the six points selected in the calculation area. Since

there were many cases, working conditions 1, 5, and 9 were selected as representatives. The temperature profile curves of each point under the three working conditions, shown in Figure 4, and the calculation data of each case revealed that the temperature change trend of the same point is basically the same in different cases.

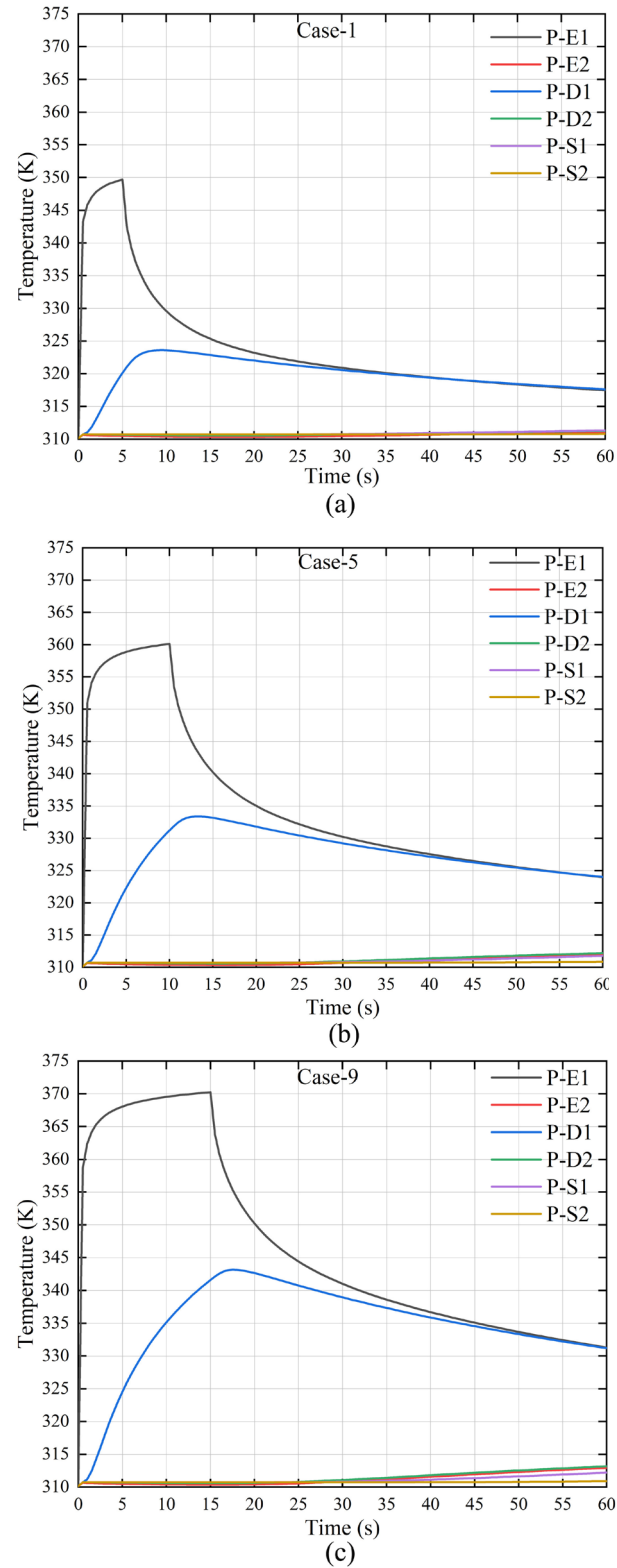


Figure 4. Temperature profile curves of each monitoring point. (a) Case 1; (b) case 5; (c) case 9.

E1 and D1 directly below the heat source are greatly affected by the external heat source, while the temperature changes at the other four points are small in each case. This is due to the close proximity of points E1 and D1 to the heat source, which facilitates heat transfer. According to the law of the temperature profile curve, the closer to the heat source, the higher the heat transfer efficiency. The temperature of point E1 reaches more than 95% of the heat source temperature within 1 s of the activation of the heat source. When the heat source is no longer active, the temperature of E1 reaches its highest point, and then drops rapidly due to natural heat dissipation. The point D1 is farther away from the heat source than E1, the temperature profile rate is significantly lower than that at E1 due to the heat transfer resistance, and the peak temperature is also much lower than that at E1. The peak time point lags behind that at E1 and appears within 2.5~4.5 s after the heat source is no longer active. Although point S1 is directly below the heat source, heat is difficult to transfer to this point and the temperature profiles slow due to the hindrance of the three-layer thermal resistance. The other three points are located 5 mm away from the heat source in the horizontal direction, and are in a state of natural convection heat dissipation directly above, so these three points are less affected by the heat source. However, as can also be seen, the temperature profile rate at the three points is inversely proportional to the length of the heat transfer path.

Thus, as the temperature profile at individual points cannot represent the influence of the heat source on each layer of skin, the average temperature of the epidermis, dermis, and subcutaneous tissue were monitored separately and the changes in the average temperature of each layer in nine cases are shown in Figure 5. The average temperature of both the epidermis and dermis showed a rapid rise under the action of the heat source, and gradually decreased after the heat source was no longer active. The highest temperatures reached by both occurred in case 9, with the highest values of 343.7 and 328.5 K, respectively. The subcutaneous tissue is insulated by the epidermis and dermis, and was less affected by the heat source, with a maximum temperature of only 313.3 K.

The temperature changes of each point of each layer are illustrated more intuitively in Figure 6, which shows the temperature field distribution of the working conditions at different times. For comparison purposes, cases 3, 6, and 9, with a heat source action time of 15 s and a heat source temperature of 353, 363, and 373 K, respectively, were selected as representative cases. At the same heat source temperature, the area of the affected region, whose temperature profiles significantly increase with action time, and the rate of downward heat transfer are higher than those to the right. The reason for this phenomenon is that the skin surface on the right side dissipates heat to the environment and is far away from the heat source. When the heat source turns into natural convection heat dissipation, the skin temperature first drops rapidly, and then the temperature of other regions also shows a downward trend. At the same action time, the higher the temperature of the heat source, the faster the heating rate of the skin and the larger the affected area; in particular, the epidermis, which is closest to the heat source, is affected the fastest and most directly. The distribution law of the temperature field shown in Figure 6 is also consistent with the temperature change trend shown in Figures 4 and 5.

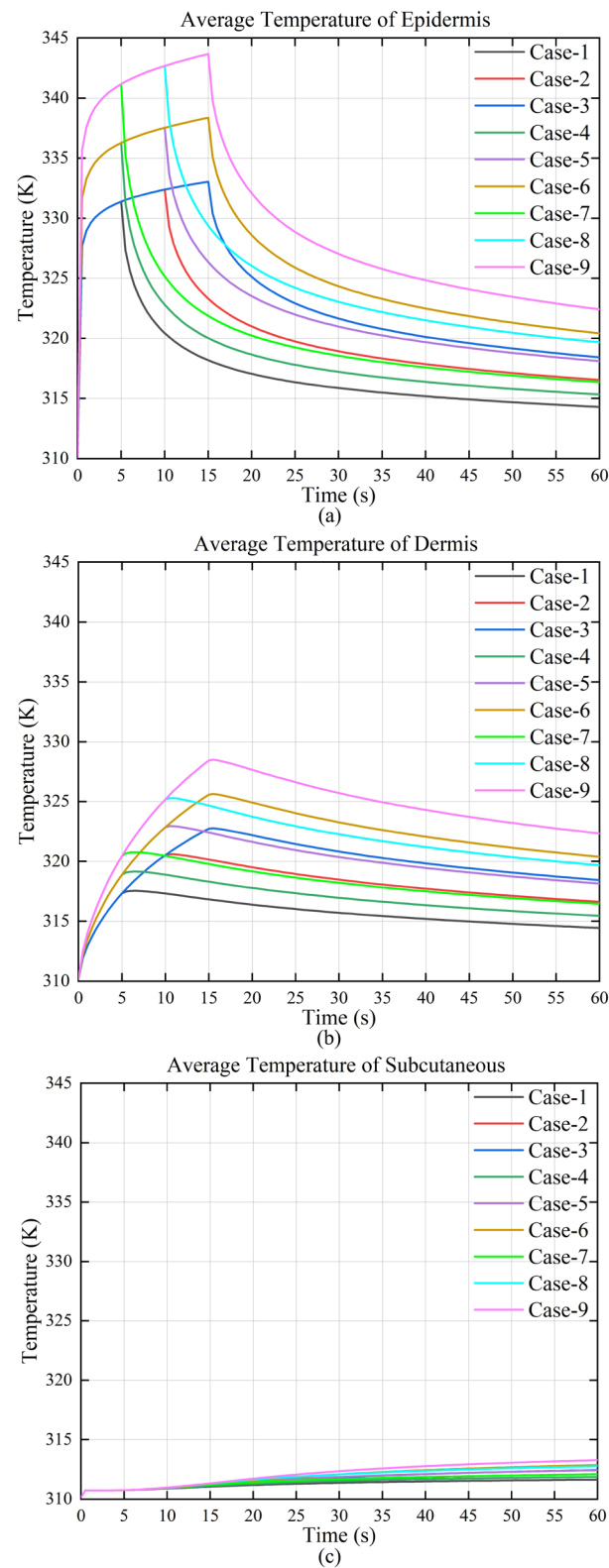


Figure 5. Changes in the average temperature of each layer under various conditions. (a) Average temperature of the epidermis; (b) average temperature of the dermis; and (c) average temperature of subcutaneous tissue.

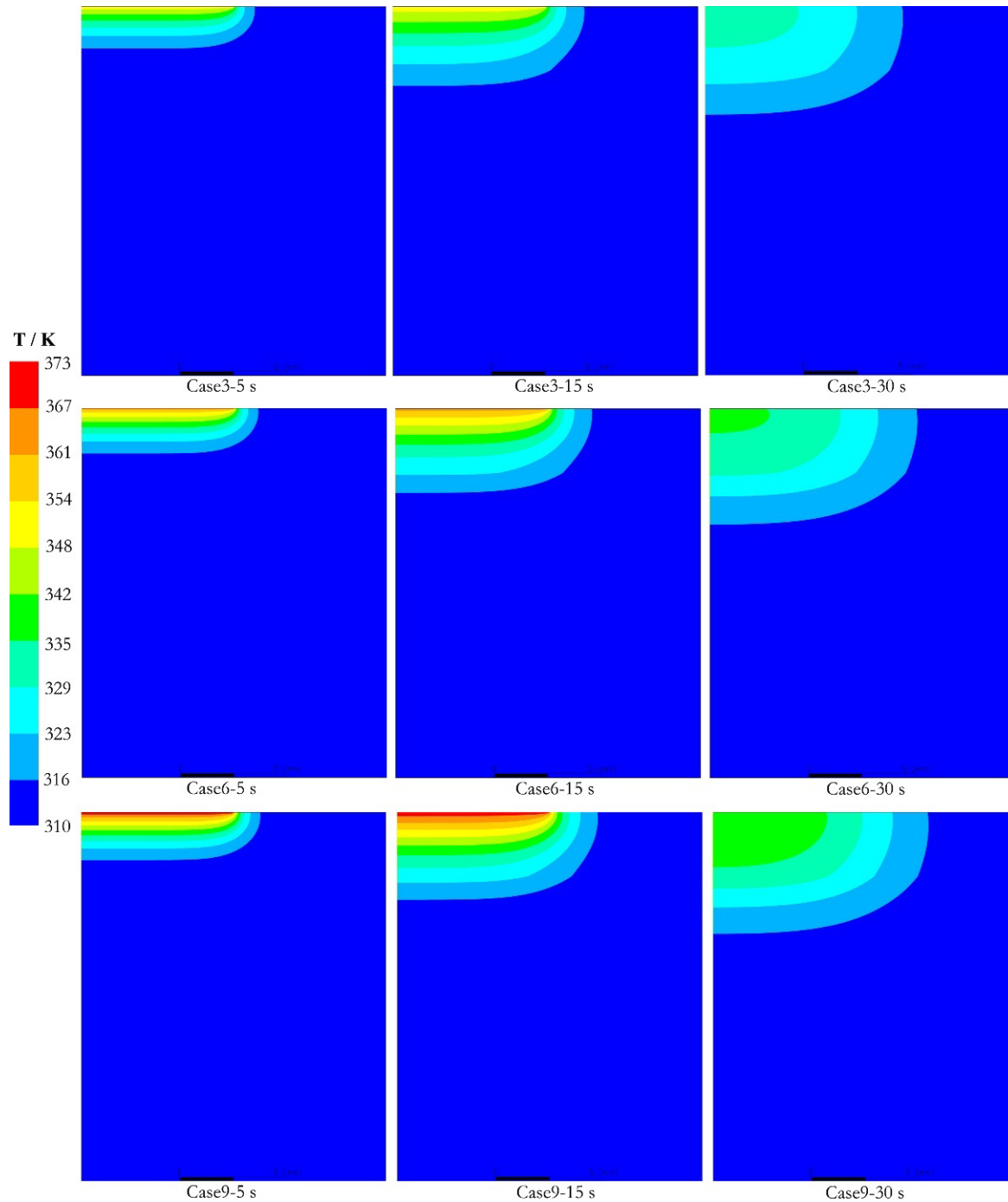


Figure 6. Temperature field distribution under cases 3, 6, and 9 at different times.

3.3. Effect of the Heat Source on the Damage Integral Distribution

Since the skin burn is not only affected by the temperature, but is also closely related to the action time, it is necessary to calculate and analyze the damage integral value Ω . The monitoring of the damage integral value Ω was also performed on the six points selected in the calculation area, and it was found that the points S1, E2, D2, and S2 had not reached the initial temperature of damage in each case and the damage integral value was always zero. Therefore, it is only necessary to plot the burn damage integral values of at points E1 and D1 in each case, as shown in Figure 7. Due to the large value, the logarithmic scale is used.

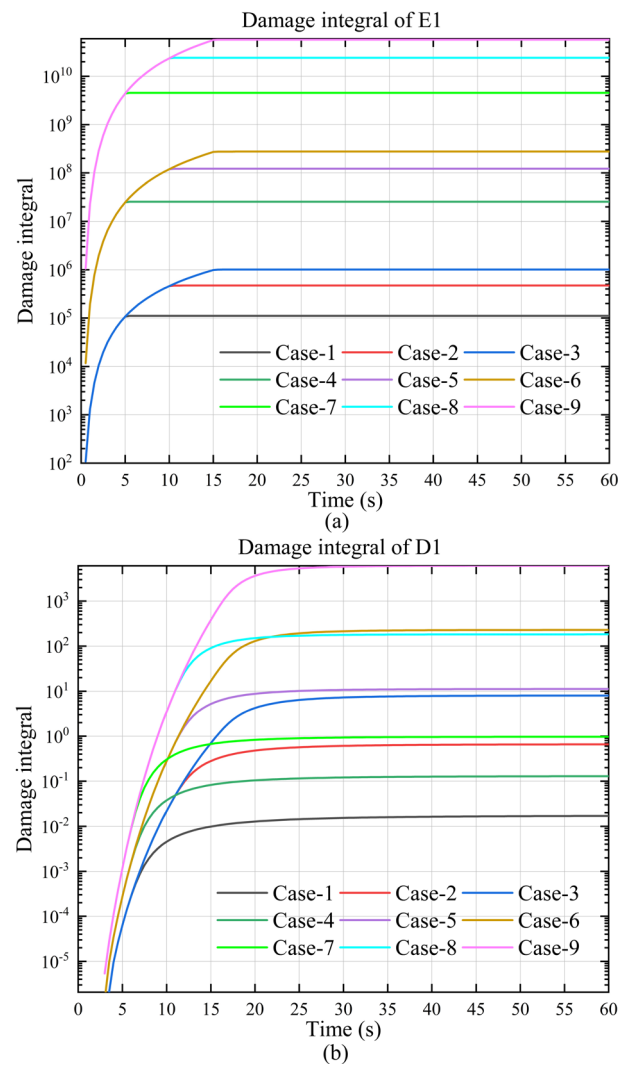


Figure 7. The change law of burn damage integral value with time in each case. (a) Damage integral value at E1; (b) damage integral value at point D1.

The plots in Figure 7 reveal that the burn damage integral value is very sensitive to temperature and point E1 is most affected as it is close to the heat source. When the heat source is 373 K, the highest burn damage integral value can reach 1011, which is two and four orders of magnitude higher than that of the heat source at 363 K and 373 K, respectively. Point D1 is less affected by the heat source than point E1, and the highest burn damage integral value is only about 6000, which is seven orders of magnitude lower than the highest value at point E1, and the gap is very large. A comparison of the burn damage integral values at point E1 in various cases revealed that when the temperature is high, the burn damage integral value rises rapidly in a short period of time. For example, the comparison between case 7 and case 6 revealed that the burn damage integral value generated by the heat source temperature of 373 K for 5 s on point E1 was much higher than that of the heat source at 363 K for 15 s. In the case of relatively low temperature, the damage integral is not only affected by the temperature, but also by the action time. For example, the comparison between case 8 and case 6 showed that the damage integral value generated by the heat source temperature of 373 K for 10 s on point D1 was slightly lower than that of the heat source at 363 K for 15 s.

The plots in Figure 7 also show that although the burn damage integral value is greatly affected by temperature, the burn damage integral value of individual points cannot represent the effect of the heat source on each layer of skin. Therefore, the average burn

damage integral values of the epidermis, dermis, and subcutaneous tissue were monitored separately, and the changes in the average burn damage integral values of each layer in nine cases are shown in Figure 8. The epidermis and dermis were severely affected as they were closer to the heat source, and the average burn damage integral value increased with the increase in the action time, and the value remained unchanged after the heat source was no longer active. An increase in the temperature of the heat source can cause a rapid increase in the average burn damage integral value, and the increase is inversely proportional to the depth. The subcutaneous tissue was affected by heat transfer lag and the average value showed a rising trend with the increase in the heat source temperature and time. However, despite this rising trend, the highest average burn damage integral value of the subcutaneous tissue was only about 0.1, which did not reach the level of burns. For the dermis and epidermis, the lowest average burn damage integral value exceeded 10² and 10⁵, respectively, and the burn damage reached second- and third-degree burns.

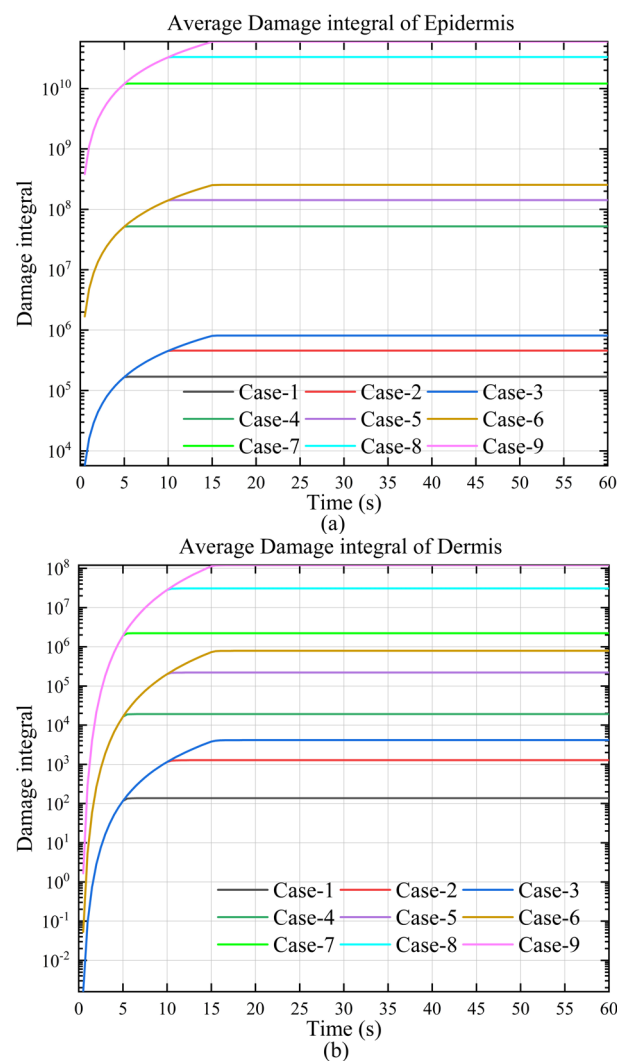


Figure 8. Cont.

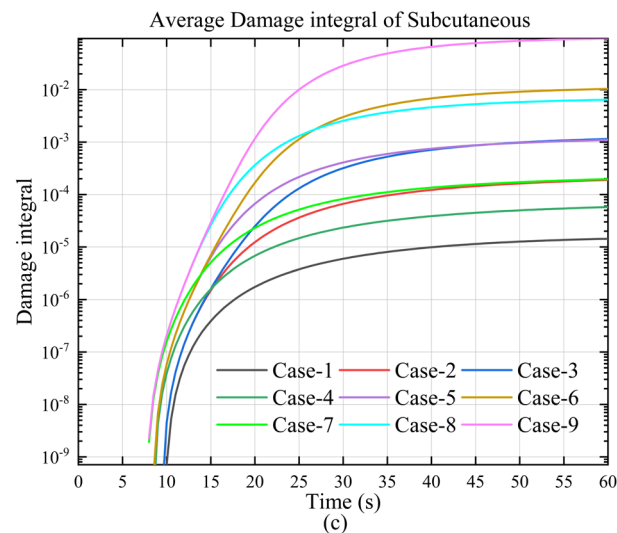


Figure 8. The change law of the average burn damage integral value of each layer over time. (a) Average burn damage integral value of the epidermis; (b) average burn damage integral value of the dermis; and (c) average burn damage integral value of subcutaneous tissue.

In order to illustrate the changes in the integral value of the burn damage at each point of each layer more intuitively, Figure 9 shows the distribution of burn damage integral values in different cases at different times. For comparison purposes, cases 2, 5, and 8, with a heat source action time of 10 s and a heat source temperature of 363 K and 373 K, respectively, were selected as representatives. At the same heat source temperature, the area of damage gradually expands with time. Unlike the tendency of the upper skin temperature to drop immediately after the heat source is no longer active, the area of the damaged region will continue to expand for a period of time even after the heat source is no longer active. The reason for this is that the skin damage is irreversible. Even if the temperature of the upper layer drops, it will not cause a drop in the burn damage integral value of the area. However, the lower layer is still affected by heat transfer and will not immediately cool down to a safe temperature; thus, tissue damage will continue to occur for a period of time after the heat source is no longer active, until the temperature of the entire area drops below the safe temperature. In the same action time, the higher the heat source temperature, the larger the skin damage area, and the burn damage integral value increases sharply with the increase in the heat source temperature. This trend is also consistent with the temperature field distribution law shown in Figure 6.

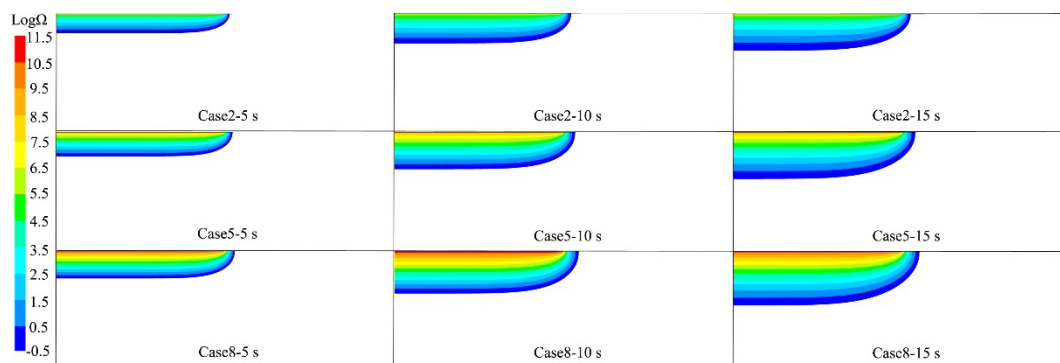


Figure 9. Distribution of damage integral values under cases 2, 5, and 8 at different times.

3.4. Effect of the Heat Source on the Burn Degree

Although Figure 9 shows the damage integral values of each layer under the action of different heat sources for different times, it is difficult to directly monitor the real-time burn degree of the skin because some values are very large under the condition of high temperature. To more clearly distinguish the real-time skin burn degree, the temperature of the heat source was selected to be 363 K and 373 K, respectively. The division of the burn degree area when the action time is 15 s, shown in Figure 9, reveals that at the same action time, the total damage area increases with the increase in heat source temperature, and this trend is consistent with the distribution law of the burn damage integral value shown in Figure 10. It should be emphasized that the area of the most severe third-degree burn damage increased the fastest, while the second-degree and first-degree damage areas increased at a slower rate. In particular, the area of the first-degree damage not only grew very slowly, but its own area was also very small compared with the areas of the third-degree and second-degree damage. Thus, it can be inferred from these findings that when the heat source temperature is high, the areas of the third-degree and second-degree burn damage are relatively large, while the area of the first-degree damage is small, that is, the damage is more serious.

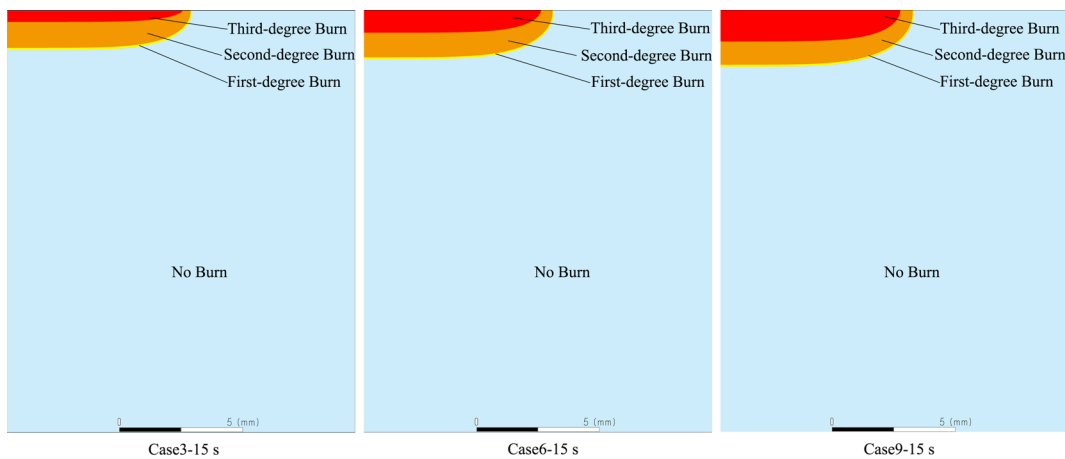


Figure 10. Regional division of each burn degree in three cases.

The distribution of burn degrees in the three cases at the same heat source action time is shown in Figure 10, but it is impossible to compare the change in each burn degree over time. In order to simply and intuitively display the temperature distribution and burn grade distribution, the previous pictures all use two-dimensional images. However, the calculation model we selected is a three-dimensional model, so when we calculate the proportion of each burn grade in the subsequent calculation, we use volume proportion for data analysis. The ratios of the volume of the three burn degrees to the total volume over time in the respective cases, shown in Figure 11, indicate that in the respective cases, the damage volume of each burn degree increases with time and the increase rate shows a downward trend, but the damage volume of the third-degree burn basically does not change after 20 s. This is because the temperature required to cause the third-degree burn is relatively high, and it is difficult to continue to expand the volume of the third-degree burn after the heat source is no longer active. Thus, it can be inferred that the size of the second-degree and first-degree burns will gradually stabilize with the extension of time. The skin damage caused by the increase in the heat source temperature is mainly reflected in the rapid increase in the volume of the third-degree burn in the early stage of injury, but has little effect on the volume of second-degree and first-degree burns. Although the increase in the heat source temperature will aggravate the expansion of the burn volume

of all degrees, the ratio of burn to total volume is still relatively small. For example, the volume proportions of the first-, second- and third-degree damage volume in 60 s were 0.4, 2.9 and 1.9%, respectively, and the sum of the total burn volume proportions was only 5.2%. Together with Figures 10 and 11, various specific parameters such as the position, depth, and volume of various burn degrees caused in different cases can be accurately predicted, providing a scientific basis for precise treatment.

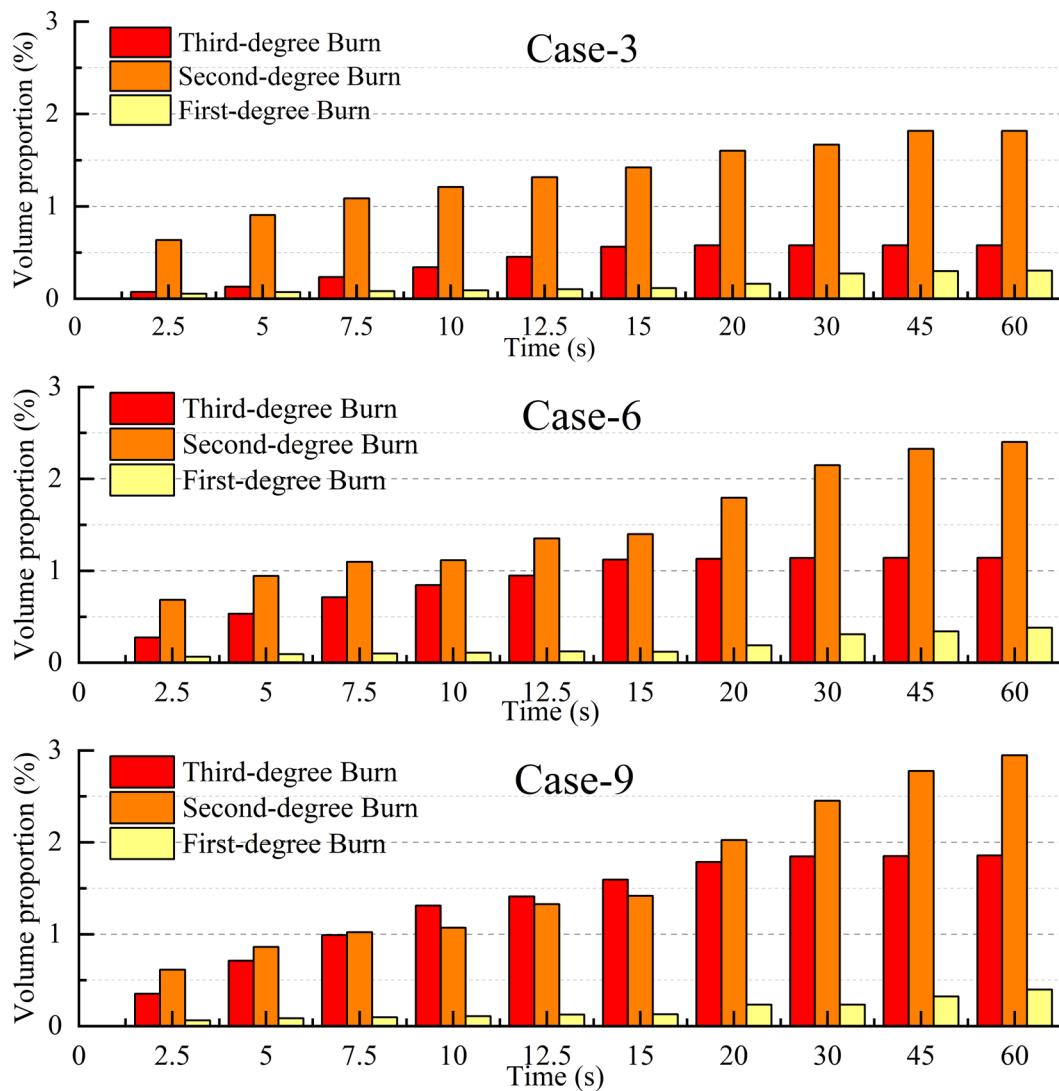


Figure 11. The proportion of the damage volume of each burn degree changes with time in three cases.

4. Conclusions

In this study, the C programming language was used to program a user defined function of the burn damage integral formula, and the coupling numerical simulation method was used to calculate the heat transfer and the burn damage integral value in a high-temperature water burn process. Then, the temperature and damage integral value at each point could be obtained to accurately assess and distinguish the burn degree in real time, and predict the position distribution, volume size, and transient change trend of each burn degree. It was determined that the heat source mainly affected the epidermis and dermis directly below, and had less effect on the area above, which is in convective heat transfer. After being heated by hot water at 373 K for 1 s, the temperature at the center of the epidermis was close to 363 K, and the temperature profile at the boundary of the same depth did not exceed 3 °C, even if it was heated for 15 s. Due to the heat transfer delay at

the center of the dermis, the temperature reached a peak value of 343 K in about 3.5 s after the heat source was no longer active. Under the protection of the epidermis and dermis, the average temperature profile of the subcutaneous tissue was also less than 3 K. The burn damage integral value was very sensitive to temperature, and the highest burn damage integral value caused by 373 K was two and four orders of magnitude higher than that caused by 363 and 353 K, respectively. The total volume of skin damage increases with the increase in the heat source temperature and the prolongation of the action time. The skin damage caused by the increase in the heat source temperature was mainly reflected in the rapid increase in the volume of the third-degree burn in the early stage of injury, but had little effect on the volume of the second- and first-degree burns. After the heat source was no longer active, the volume of the third-, second- and first-degree burns gradually stabilized. Although some damaged volume had a large increase, the total volume accounted for only a small proportion. After heating at 373 K for 15 s and continuing to delay the action for 45 s, the volume of first-, second-, and third-degree burns accounted for 0.4, 2.9, and 1.9%, respectively, and the total volume of damage accounted for only 5.2% of the total volume.

Author Contributions: Conceptualization, C.Z. and J.L.; data curation, X.M.; formal analysis, C.Z.; funding acquisition, J.L.; investigation, C.Z., X.M. and Y.Q.; methodology, C.Z.; project administration, J.L.; software, C.Z.; supervision, M.L., M.K.K. and J.L.; validation, C.Z. and M.L.; visualization, M.L. and M.K.K.; writing—original draft, C.Z.; writing—review and editing, C.Z., X.M., M.L., Y.Q., M.K.K. and J.L. All authors have read and agreed to the published version of the manuscript.

Funding: This research was funded by the Doctoral Research Fund of Shandong Jianzhu University, grant number X21020Z; the Research Fund of Shandong University of Engineering and Vocational Technology, grant number SDGCS2108; and the Shandong Province Art Science Key Project, grant number L2022Q06170107.

Data Availability Statement: The data presented in this study are available on request from the corresponding author.

Acknowledgments: This work was also supported by the Plan of Introduction and Cultivation for Young Innovative Talents in Colleges and Universities of Shandong Province.

Conflicts of Interest: The authors declare no conflicts of interest.

Nomenclature

c_b	Specific heat of blood ($J \cdot kg^{-1} \cdot K^{-1}$)
c_s	Specific heat of skin tissue ($J \cdot kg^{-1} \cdot K^{-1}$)
d_1	Thickness of epidermis (mm)
D_1	Monitoring location point D_1
d_2	Thickness of dermis (mm)
D_2	Monitoring location point D_2
d_3	Thickness of subcutaneous tissue (mm)
E_1	Monitoring location point E_1
E_2	Monitoring location point E_2
h	Convection transfer rate ($W \cdot m^{-2} \cdot K^{-1}$)
P	Pre-exponential frequency factor (s^{-1})
Q_b	Blood perfusion heat ($W \cdot m^{-3}$)
Q_{met}	Metabolism heat ($W \cdot m^{-3}$)
r_{hs}	Radius of heat source (mm)
r_{pm}	Radius of physical model (mm)
R	Molar gas constant ($J \cdot mol^{-1} \cdot K^{-1}$)
S_1	Monitoring location point S_1
S_2	Monitoring location point S_2

T_b	Blood temperature (K)
T_∞	Ambient temperature of the atmosphere (K)
z_{pm}	Thickness of physical model (mm)
ΔE	Apparent activation energy ($\text{J} \cdot \text{mol}^{-1}$)
■	The burn damage integral value
ρ_b	Density of blood ($\text{kg} \cdot \text{m}^{-3}$)
ρ_s	Density of skin tissue ($\text{kg} \cdot \text{m}^{-3}$)
τ_{hs}	Duration of heat source (s)
ω_b	Blood perfusion rate ($\text{m}^3 \cdot \text{s}^{-1}$)
λ_s	Thermal conductivity of skin tissue ($\text{W} \cdot \text{m}^{-1} \cdot \text{K}^{-1}$)

References

- Kankam, H.K.N.; Lee, K.C.; Sardeli, A.V.; Dretzke, J.; Lord, J.M.; Moiemmen, N. Acute burn injuries associated with long-term mortality: A systematic review and meta-analysis. *Burns* **2022**, *48*, 1783–1793. [[CrossRef](#)] [[PubMed](#)]
- Schoenbrunner, A.; Banda, W.; Gosman, A.A. Global Burn Care: Education and Research. *Clin. Plast. Surg.* **2017**, *44*, 485–493. [[CrossRef](#)] [[PubMed](#)]
- Banga, A.T.; Westgarth-Taylor, C.; Grieve, A. The Epidemiology of Paediatric Burn Injuries in Johannesburg, South Africa. *J. Pediatr. Surg.* **2023**, *58*, 287–292. [[CrossRef](#)] [[PubMed](#)]
- Hop, M.J.; Wijnen, B.F.; Nieuwenhuis, M.K.; Dokter, J.; Middelkoop, E.; Polinder, S.; van Baar, M.E.; Dutch Burn Repository Group. Economic burden of burn injuries in the Netherlands: A 3 months follow-up study. *Injury* **2016**, *47*, 203–210. [[CrossRef](#)]
- Hultman, C.S.; van Duin, D.; Sickbert-Bennett, E.; DiBiase, L.M.; Jones, S.W.; Cairns, B.A.; Weber, D.J. Systems-based Practice in Burn Care: Prevention, Management, and Economic Impact of Health Care-associated Infections. *Clin. Plast. Surg.* **2017**, *44*, 935–942. [[CrossRef](#)]
- Pennes, H.H. Analysis of tissue and arterial blood temperatures in the resting human forearm. *J. Appl. Physiol.* **1948**, *1*, 93–122. [[CrossRef](#)]
- Diller, K.R.; Hayes, L.J.; Baxter, C.R. A mathematical model for the thermal efficacy of cooling therapy for burns. *J. Burn Care Rehabil.* **1983**, *4*, 81–89. [[CrossRef](#)]
- Prinzmetal, M.; Bergman, H.C.; Kruger, H.E. Demonstration of a Toxic Factor in the Blood of Rats Shocked by Burn. *J. Clin. Investig.* **1946**, *25*, 781–784. [[CrossRef](#)]
- Henriques, F.C., Jr.; Moritz, A.R. Studies of thermal injury II. The relative importance of time and surface temperature in the causation of cutaneous burns. *Am. J. Pathol.* **1947**, *23*, 695–720.
- Mansilla, E.; Spretz, R.; Larsen, G.; Nuñez, L.; Drago, H.; Sturla, F.; Marin, G.H.; Roque, G.; Martire, K.; Díaz Aquino, V.; et al. Outstanding Survival and Regeneration Process by the Use of Intelligent Acellular Dermal Matrices and Mesenchymal Stem Cells in a Burn Pig Model. *Transplant. Proc.* **2010**, *42*, 4275–4278. [[CrossRef](#)]
- Sheu, S.Y.; Wang, W.L.; Fu, Y.T.; Lin, S.C.; Lei, Y.C.; Liao, J.H.; Tang, N.Y.; Kuo, T.F.; Yao, C.H. The pig as an experimental model for mid-dermal burns research. *Burns* **2014**, *40*, 1679–1688. [[CrossRef](#)] [[PubMed](#)]
- Zhuravleva, K.; Goertz, O.; Wölkart, G.; Guillemot, L.; Petzelbauer, P.; Lehnhardt, M.; Schmidt, K.; Citi, S.; Schossleitner, K. The tight junction protein cingulin regulates the vascular response to burn injury in a mouse model. *Microvasc. Res.* **2020**, *132*, 104067. [[CrossRef](#)] [[PubMed](#)]
- Zhao, Y.; Liu, J.; Ding, Z.; Ge, W.; Wang, S.; Zhang, J. ATP-induced hypothermia improves burn injury and relieves burn pain in mice. *J. Therm. Biol.* **2023**, *114*, 103563. [[CrossRef](#)]
- Chen, L.; Xie, L.; Tan, J.; Li, N.; Luo, Y.; Li, M.; Zhang, S.; Wang, Z. The gut microbiota regulates the depressive-type behaviors and inflammatory processes after severe burn injuries in mice. *Heliyon* **2024**, *10*, e25617. [[CrossRef](#)] [[PubMed](#)]
- Hu, R.H.; Yu, Y.M.; Costa, D.; Young, V.R.; Ryan, C.M.; Burke, J.F.; Tompkins, R.G. A rabbit model for metabolic studies after burn injury. *J. Surg. Res.* **1998**, *75*, 153–160. [[CrossRef](#)]
- Defagó, V.; Moyano, J.; Bernhardt, C.; Sambuelli, G.; Cuestas, E. Protective effect of early placement of nasogastric tube with solid dilator on tissue damage and stricture formation after caustic esophageal burns in rabbits. *J. Pediatr. Surg.* **2015**, *50*, 1264–1268. [[CrossRef](#)]
- Ozcan, O.; Ipekci, H.; Alev, B.; Ustundag, U.V.; Sen, A.; Emekli-Alturfan, E.; Sener, G.; Yarat, A.; Tunali-Akbay, T. The effect of *Myrtus communis* L. ethanol extract on the small intestine and lungs in experimental thermal burn injury. *J. Therm. Biol.* **2020**, *93*, 102685. [[CrossRef](#)]
- Mulder, P.P.G.; Koenen, H.J.P.M.; Vlig, M.; Joosten, I.; de Vries, R.B.M.; Boekema, B.K.H.L. Burn-Induced Local and Systemic Immune Response: Systematic Review and Meta-Analysis of Animal Studies. *J. Investig. Dermatol.* **2022**, *142*, 3093–3109. [[CrossRef](#)]

19. Sasaki, M.; Abe, R.; Fujita, Y.; Ando, S.; Inokuma, D.; Shimizu, H. Mesenchymal stem cells are recruited into wounded skin and contribute to wound repair by transdifferentiation into multiple skin cell type. *J. Immunol.* **2008**, *180*, 2581–2587. [[CrossRef](#)]
20. Lewis, C.J. Stem cell application in acute burn care and reconstruction. *J. Wound Care* **2013**, *22*, 7–16. [[CrossRef](#)]
21. Ehrenreich, M.; Ruszczak, Z. Tissue-engineered temporary wound coverings. Important options for the clinician. *Acta Dermatovenerol. Alp. Pannonica Adriat.* **2006**, *15*, 5–13. [[PubMed](#)]
22. Hermans, M.H. Preservation methods of allografts and their (lack of) influence on clinical results in partial thickness burns. *Burns* **2011**, *37*, 873–881. [[CrossRef](#)] [[PubMed](#)]
23. Graca, M.F.P.; Miguel, S.P.; Cabral, C.S.D.; Correia, I.J. Hyaluronic acid-Based wound dressings: A review. *Carbohydr. Polym.* **2020**, *241*, 116364. [[CrossRef](#)] [[PubMed](#)]
24. Pepliński, B. External Costs for Agriculture from Lignite Extraction from the Złoczew Deposit. *Energies* **2021**, *14*, 2660. [[CrossRef](#)]
25. Baldwin, A.; Xu, J.; Attinger, D. How to cool a burn: A heat transfer point of view. *J. Burn Care Res.* **2012**, *33*, 176–187. [[CrossRef](#)]
26. Ali, A.; Bukhari, Z.; Shahzadi, G.; Abbas, Z.; Umar, M. Numerical Simulation of the Thermally Developed Pulsatile Flow of a Hybrid Nanofluid in a Constricted Channel. *Energies* **2021**, *14*, 2410. [[CrossRef](#)]
27. Csenkey, A.; Hargitai, E.; Pakai, E.; Kajtar, B.; Vida, L.; Lorincz, A.; Gergics, M.; Vajda, P.; Jozsa, G.; Garami, A. Effectiveness of four topical treatment methods in a rat model of superficial partial-thickness burn injury: The advantages of combining zinc-hyaluronan gel with silver foam dressing. *Injury* **2022**, *53*, 3912–3919. [[CrossRef](#)]
28. Ng, E.Y.; Chua, L.T. Mesh-independent prediction of skin burns injury. *J. Med. Eng. Technol.* **2000**, *24*, 255–261.
29. Ng, E.Y.; Chua, L.T. Prediction of skin burn injury. Part 1: Numerical modelling. *Proc. Inst. Mech. Eng. H* **2002**, *216*, 157–170. [[CrossRef](#)]
30. Ng, E.Y.; Chua, L.T. Prediction of skin burn injury. Part 2: Parametric and sensitivity analysis. *Proc. Inst. Mech. Eng. H* **2002**, *216*, 171–183. [[CrossRef](#)]
31. Abraham, J.P.; Plourde, B.; Vallez, L.; Stark, J.; Diller, K.R. Estimating the time and temperature relationship for causation of deep-partial thickness skin burns. *Burns* **2015**, *41*, 1741–1747. [[CrossRef](#)] [[PubMed](#)]
32. Dai, W.; Wang, H.; Jordan, P.M.; Mickens, R.E.; Bejan, A. A mathematical model for skin burn injury induced by radiation heating. *Int. J. Heat Mass Transf.* **2008**, *51*, 5497–5510. [[CrossRef](#)]
33. Ng, E.Y.K.; Tan, H.M.; Ooi, E.H. Boundary element method with bioheat equation for skin burn injury. *Burns* **2009**, *35*, 987–997. [[CrossRef](#)] [[PubMed](#)]
34. Etehadtavakol, M.; Ng, E.Y.K. Survey of numerical bioheat transfer modelling for accurate skin surface measurements. *Therm. Sci. Eng. Prog.* **2020**, *20*, 100681. [[CrossRef](#)]
35. Jiang, S.C.; Ma, N.; Li, H.J.; Zhang, X.X. Effects of thermal properties and geometrical dimensions on skin burn injuries. *Burns* **2002**, *28*, 713–717. [[CrossRef](#)]
36. Malekmohamadi, M.H.; Ahmadikia, H.; Mosharaf-Dehkordi, M. The effect of heat flux distribution and internal heat generation on the thermal damage in multilayer tissue in thermotherapy. *J. Therm. Biol.* **2021**, *99*, 102920. [[CrossRef](#)]
37. Kashcooli, M.; Salimpour, M.R.; Shirani, E. Heat transfer analysis of skin during thermal therapy using thermal wave equation. *J. Therm. Biol.* **2017**, *64*, 7–18. [[CrossRef](#)]
38. Lee, S.L.; Lu, Y.H. Modeling of bioheat equation for skin and a preliminary study on a noninvasive diagnostic method for skin burn wounds. *Burns* **2014**, *40*, 930–939. [[CrossRef](#)]
39. Wang, Z.; Zhao, G.; Wang, T.; Yu, Q.; Su, M.; He, X. Three-dimensional numerical simulation of the effects of fractal vascular trees on tissue temperature and intracellular ice formation during combined cancer therapy of cryosurgery and hyperthermia. *Appl. Therm. Eng.* **2015**, *90*, 296–304. [[CrossRef](#)]
40. Shirkavand, A.; Nazif, H.R. Numerical study on the effects of blood perfusion and body metabolism on the temperature profile of human forearm in hyperthermia conditions. *J. Therm. Biol.* **2019**, *84*, 339–350. [[CrossRef](#)]
41. Muddassir, M.; Limbert, G.; Navarro-Alarcon, D. Development of a numerical multi-layer model of skin subjected to pulsed laser irradiation to optimise thermal stimulation in photorejuvenation procedure. *Comput. Methods Programs Biomed.* **2022**, *216*, 106653. [[CrossRef](#)] [[PubMed](#)]
42. Wu, J.; Hu, Z.; Gu, Y.; Li, L.; Zhu, H. A multi-segmented human bioheat model for cold and extremely cold exposures. *Int. J. Therm. Sci.* **2022**, *173*, 107394. [[CrossRef](#)]
43. Dinda, A.; Acharya, J.; Bhanja, D.; Nath, S. Local thermal non-equilibrium bioheat transfer model for interstitial hyperthermia treatment of tumour cell: A numerical approach. *J. Therm. Biol.* **2022**, *110*, 103368. [[CrossRef](#)] [[PubMed](#)]
44. Log, T. Modeling Skin Injury from Hot Spills on Clothing. *Int. J. Environ. Res. Public Health* **2017**, *14*, 1374. [[CrossRef](#)]
45. Log, T. Modeling Burns for Pre-Cooled Skin Flame Exposure. *Int. J. Environ. Res. Public Health* **2017**, *14*, 1024. [[CrossRef](#)]
46. Log, T. Modeling Skin Injury from Hot Rice Porridge Spills. *Int. J. Environ. Res. Public Health* **2018**, *15*, 808. [[CrossRef](#)]
47. Zhang, Q.; Sun, Y.; Yang, J. Thermoelastic behavior of skin tissue induced by laser irradiation based on the generalized dual-phase lag model. *J. Therm. Biol.* **2021**, *100*, 103038. [[CrossRef](#)]

48. Lu, X.; Meng, J.; Chen, G.; Lu, Y. Numerical simulation of heat and moisture transfer in protective clothing under high pressure steam exposure: Effect of fabric properties and steam conditions. *Int. J. Therm. Sci.* **2023**, *194*, 108550. [[CrossRef](#)]
49. Yang, J.; Zhang, S. Three-dimensional simulation of the convective heat transfer coefficient of the human body under various air velocities and human body angles. *Int. J. Therm. Sci.* **2023**, *187*, 108171. [[CrossRef](#)]
50. Wang, Y.; Xu, Y.; Xu, D.; Fan, J. The heat and moisture transfer model of firefighter protective clothing. *Int. J. Therm. Sci.* **2024**, *197*, 108854. [[CrossRef](#)]

Disclaimer/Publisher's Note: The statements, opinions and data contained in all publications are solely those of the individual author(s) and contributor(s) and not of MDPI and/or the editor(s). MDPI and/or the editor(s) disclaim responsibility for any injury to people or property resulting from any ideas, methods, instructions or products referred to in the content.